

1 **Revision 2**

2

3 **Synthesis of large wadsleyite single crystals by solid-state recrystallization**

4

5

6 Takaaki Kawazoe^{1*} (takaaki.kawazoe@uni-bayreuth.de),

7 Johannes Buchen¹ (johannes.buchen@uni-bayreuth.de) and

8 Hauke Marquardt¹ (hauke.marquardt@uni-bayreuth.de)

9

10 ¹Bayerisches Geoinstitut, University of Bayreuth, 95440 Bayreuth, Germany

11

12

13

14 * Corresponding author:

15 Takaaki Kawazoe

16 Tel: +49-921-55-3745

17 Fax: +49-921-55-3769

18

ABSTRACT

19 Single crystals of $(\text{Mg}_{0.89}\text{Fe}_{0.11})_2\text{SiO}_4$ wadsleyite with dimensions up to ~1 mm were
20 synthesized by solid-state recrystallization under high pressure. Synthesis experiments of the
21 wadsleyite single crystals were performed at 16 GPa and 1870 K for 1–3 h using a Kawai-type
22 multianvil apparatus. The wadsleyite crystals are virtually free of inclusions and cracks. Their
23 chemical compositions are homogeneous with $\text{Fe}/(\text{Mg} + \text{Fe})$ of 0.112(2). Unpolarized infrared
24 spectra indicate that the synthesized sample contains 0.15-0.30 wt% H_2O . The method of
25 synthesizing large, high-quality single crystals of wadsleyite will facilitate future measurements of
26 physical properties including elasticity and elastic anisotropy, electrical and thermal conductivities, atomic
27 diffusivity and creep strength, which will improve models of the composition and dynamics of the mantle
28 transition zone.

29

30 **Keywords:** wadsleyite, single crystal, mantle transition zone, high-pressure synthesis,
31 Kawai-type multianvil apparatus

32

33

INTRODUCTION

34 Wadsleyite is expected to be the most dominant mineral at the upper part of the mantle
35 transition zone (MTZ) (e.g. Irifune and Isshiki 1998) and thereby controls the physical and
36 chemical properties of this region. Seismic observations have revealed anisotropic seismic wave
37 propagation within the upper MTZ (e.g. Visser et al. 2008). Global seismic anisotropy in the
38 upper MTZ has been attributed to a crystallographic preferred orientation (CPO) of wadsleyite
39 (e.g. Kawazoe et al. 2013). However, a quantitative evaluation of the seismic anisotropy observed
40 in the upper MTZ is difficult because the elastic stiffness constants C_{ijkl} of wadsleyite have not
41 been experimentally determined under simultaneous high pressure and high temperature (e.g.
42 Wang et al. 2014). Moreover, the wadsleyite CPO in the upper MTZ may cause anisotropy in
43 other physical properties such as viscosity; c.f. deformed olivine in the upper mantle (Hansen et
44 al. 2012). Consequently, a detailed understanding of the anisotropy of the physical properties of
45 wadsleyite is fundamental to model anisotropy of physical and chemical properties in the upper
46 MTZ.

47 Many types of experiments to determine anisotropy in physical and chemical properties
48 of wadsleyite require single crystals of sufficient size and quality. In experiments with diamond
49 anvil cells (DAC), single crystals larger than 100 μm are useful for the preparation of
50 single-crystal samples with defined dimensions, shape and if needed crystallographic orientation

51 by the focused ion beam (FIB) technique (Marquardt and Marquardt 2012). In the case of
52 multianvil apparatuses, atomic diffusion and deformation experiments can be performed on
53 wadsleyite samples as small as 0.4–0.5 mm (Kawazoe et al. 2010; Shimojuku et al. 2004).
54 Therefore, wadsleyite single crystals larger than ~0.4 mm are ideal for a range of experiments to
55 determine the anisotropy of its physical properties under high pressure and temperature.

56 Previously, large wadsleyite single crystals were synthesized by solid-state
57 recrystallization using a Kawai-type multianvil apparatus (Sawamoto 1986). In these experiments,
58 wadsleyite single crystals with dimensions up to 0.5 mm were obtained near the
59 wadsleyite–ringwoodite phase boundary (19–21.5 GPa and 1940–2670 K). However, the
60 wadsleyite crystals contained inclusions and showed variation in Mg/(Mg + Fe) from crystal to
61 crystal (Sawamoto 1986). We note that in this previous study, temperature was overestimated
62 because it has been shown that Mg₂SiO₄ ringwoodite is unstable above ~2170 K (e.g. Fei et al.
63 2004). In another work, the temperature-gradient method was applied to single-crystal growth of
64 wadsleyite in carbonate solutions using a Kawai-type apparatus (Shatskiy et al. 2009). In these
65 experiments, wadsleyite single crystals with dimensions up to 1.0 mm were obtained in
66 co-existence with quenched melt. However, the carbonate flux method produced crystals with
67 inclusions of the solvent (Shatskiy et al. 2009).

68 In the present study, we synthesized high-quality single crystals of $(\text{Mg}_{0.89}\text{Fe}_{0.11})_2\text{SiO}_4$
69 wadsleyite with dimensions up to ~ 1 mm by solid-state recrystallization. We describe the method
70 and discuss sample characterization including evaluation of inclusions, cracks, chemical compositions
71 and water content. In addition, we outline potential applications for the synthesized crystals to
72 study the intrinsic anisotropy of wadsleyite to many physical and chemical properties.

73

74

EXPERIMENTAL METHODS

75

76 **Synthesis experiments**

77 The starting material was a powder of San Carlos olivine $((\text{Mg}_{0.9}\text{Fe}_{0.1})_2\text{SiO}_4)$. Olivine
78 single crystals with no visible inclusion were hand-picked under a stereomicroscope and ground
79 to a fine powder using a mortar. The starting powder was packed in a Re foil capsule (1.6-mm
80 outer diameter and 2.7-mm length). Neither solvent nor water was added to the starting material.

81 The high-pressure synthesis was performed using a 1000-ton Kawai-type multianvil
82 apparatus with split-sphere type guide blocks (Keppler and Frost 2005). The second-stage anvils
83 with an 8-mm truncation were made of tungsten carbide (ha-7%, hawedia). The capsule was
84 loaded into a ceramic octahedron with a 14-mm edge length made of semi-sintered Cr-doped

85 MgO. Pre-formed pyrophyllite gaskets were used. A stepped LaCrO₃ furnace was adopted with a
86 ZrO₂ thermal insulator. The ceramic parts of the cell assembly were fired at 1273 K for
87 dehydration. The sample was first compressed to 8.0 MN (815 tonf) at room temperature.
88 Temperature was then increased to 1870 K at rates of ~50-70 K/min. The generated temperature
89 was estimated based on relationships between temperature measured with a thermocouple and
90 electric power to the furnace in separate runs. The uncertainty in temperature is estimated to be
91 ±50 K. The target temperature was held for 1 h (run H4015) or 3 h (run H4150) before rapid
92 quenching. The sample was subsequently decompressed at room temperature for 13-15 h.

93

94 **Sample analyses**

95 Several crystals from both runs were examined using X-ray diffractometers with a CCD
96 area detector (Oxford Diffraction, Xcalibur2) and a point detector (Huber, SMC9000) operating
97 with Mo K α radiation (40 kV and 20-30 mA) for phase identification, verification as single crystal
98 and orientation. The quality of the crystals was evaluated based on the widths of X-ray diffraction
99 peaks in the final omega scans. Thin sections of the single crystals from run H4015 were
100 examined using a polarization microscope (Leitz, Laborlux 12 Pol S).

118 inclusions and dispersed cracks (Fig. 1c). Uniform extinction upon sample rotation under
119 cross-polarized light further indicated that the crystals were single crystals.

120 The chemical compositions of the wadsleyite crystals are nearly homogeneous within
121 each crystal and among the crystals with Fe/(Mg + Fe) of 0.112(2) (Table 1). The cations per 4
122 oxygens in Table 1 are upper bounds because ~10 % of Fe is expected to be Fe³⁺ in
123 (Mg_{0.9}Fe_{0.1})₂SiO₄ wadsleyite synthesized in the Re capsule (Frost and McCammon 2009). The
124 compositions are comparable to those expected in the upper MTZ (Irifune and Isshiki 1998).

125 The unit-cell parameters of wadsleyite from run H4015 were $a = 5.7070(9)$ and
126 $5.7069(9)$ Å, $b = 11.4735(11)$ and $11.4735(10)$ Å, and $c = 8.2741(10)$ and $8.2740(10)$ Å when the
127 orthorhombic (the space groups *Imma*, Sawamoto and Horiuchi 1990) and monoclinic (the space
128 group *I2/m*, Smyth et al. 1997) symmetries were assumed, respectively. A β angle of $90.030(11)^\circ$
129 was obtained for the monoclinic case. These cell parameters lead to unit-cell volumes of
130 $541.78(12)$ and $541.77(11)$ Å³, a density of $3.617(7)$ g/cm³, and b/a ratios of $2.0104(4)$ and
131 $2.0105(3)$ for the orthorhombic and monoclinic symmetries, respectively. The average full-width
132 at half-maximum of the final omega scans was $0.082(13)^\circ$ (Fig. 2) showing the high quality of
133 the crystals.

134 The water contents of the wadsleyite crystals parallel to the (243), (120), and (010)
135 planes were in the ranges of 0.15(1)-0.20(1), 0.22(2)-0.28(1), and 0.25(1)-0.30(1) wt% H₂O,
136 respectively (Figs. 3 and 4 and Table 2). IR absorption at 3200-3650 cm⁻¹ and the water contents
137 are consistent with the one (0.09-0.21 wt%) observed in wadsleyite synthesized from natural
138 olivine powder with no additional water in a previous study (Nishihara et al. 2006). The
139 uncertainty in the water contents given above corresponds to one standard deviation calculated
140 from measurements at 4-6 distinct locations in each single crystal, indicating the homogeneity of
141 the water content (Figs. 3 and 4). The uncertainty in absolute water content is larger than that
142 stated above and can be estimated based on the variation in water content arising from the use of
143 different calibrations (~30 %, Paterson 1982; 10-20 %, Libowitzky and Rossman 1997; 10 %,
144 Deon et al. 2010). The water was supposed to be supplied to the sample from the surrounding
145 ceramics which absorbed moisture from the air after the heating treatment (c.f. Nishihara et al.,
146 2006). This water content is comparable with that estimated for the MTZ (~0.1 wt%, Karato
147 2011).

148 Phase transformation kinetics from polycrystalline olivine to wadsleyite likely plays an
149 important role in obtaining the large wadsleyite single crystals by solid-state recrystallization.
150 The small effect of run duration on the maximum dimensions of the synthesized wadsleyite

151 crystals implies that the wadsleyite crystals primarily grew at the beginning of each run (within
152 less than 1 h). Nucleation and growth rates of wadsleyite in polycrystalline olivine significantly
153 decrease and increase with increasing temperature, respectively (Kubo et al. 2004). Therefore,
154 rapid growth of the wadsleyite crystals is expected during the olivine-wadsleyite transformation
155 because of the low nucleation density and high growth rate of wadsleyite in polycrystalline
156 olivine at high temperature.

157

158

IMPLICATIONS

159 The large size of the wadsleyite single crystals allows for preparing several samples for
160 the DAC experiments from one single crystal. As an example, we outline the potential use of the
161 crystals to determine C_{ijkl} by Brillouin spectroscopy and single-crystal X-ray diffraction. Two
162 crystals were oriented parallel to the (120) and (243) planes and double-side polished to a
163 thickness of 10 μm (Fig. 1c). Several half disks with a 110- μm diameter were cut from the
164 platelets using a FIB machine (FEI, Scios) operated at 30 kV and 7–30 nA (Fig. 1d). Two half
165 disks with different orientations were loaded with ruby and Sm-doped $\text{Y}_3\text{Al}_5\text{O}_{12}$ chips as pressure
166 calibrants in a sample chamber of a resistively heated DAC equipped with 400- μm culet
167 diamonds. The combined measurement of acoustic velocity distribution in the two chosen

168 crystallographic planes along with the measurement of unit-cell volume by X-ray diffraction
169 allows for determining all the 9 C_{ijkl} of wadsleyite at the same pressure–temperature conditions
170 (Speziale et al. 2014). The measurement enables us to minimize uncertainties related to different
171 experimental runs, such as the determination of pressure and temperature.

172 In future studies, the large high-quality single crystals will allow for determining the
173 physical properties of wadsleyite such as sound velocity anisotropy, elasticity, electrical and
174 thermal conductivities, atomic diffusivity, and creep strength. Owing to potential CPO of
175 wadsleyite (e.g. Kawazoe et al. 2013), the upper MTZ can reflect the anisotropic behavior of this
176 phase if the anisotropy in its physical properties is large enough. Consequently, further
177 applications of the grown high-quality wadsleyite single crystals are expected to contribute to the
178 advancement of high-pressure mineralogy.

179

180

ACKNOWLEDGMENTS

181 We are grateful to T. Boffa Ballaran, K. Marquardt, H. Schulze, D. Krauß, A. Potzel,
182 and H. Fischer for their supports for the X-ray diffraction, the FIB cutting, the sample polishing,
183 the chemical analysis and manufacturing the cell assembly parts, respectively. Part of this
184 research was supported through the project “GeoMaX”, funded under the Emmy-Noether

185 Program of the German Science Foundation (MA4534/3-1). We thank A. Shatskiy and S.D.
186 Jacobsen for their constructive review comments.

187

188

REFERENCES CITED

189 Deon, F., Koch-Müller, M., Rhede, D., Gottschalk, M., Wirth, R., and Thomas, S.M. (2010)

190 Location and quantification of hydroxyl in wadsleyite: New insights. American
191 Mineralogist, 95, 312-322.

192 Fei, Y., Van Orman, J.A., Li, J., Van Westrenen, W., Sanloup, C., Minarik, W., Hirose, K.,

193 Komabayashi, T., Walter, M.J., and Funakoshi, K. (2004) Experimentally determined
194 postspinel transformation boundary in Mg_2SiO_4 using MgO as an internal pressure
195 standard and its geophysical implications. Journal of Geophysical Research, 109,
196 10.1029/2003JB002562.

197 Frost, D.J., and McCammon, C.A. (2009) The effect of oxygen fugacity on the olivine to
198 wadsleyite transformation: Implications for remote sensing of mantle redox state at the
199 410 km seismic discontinuity. American Mineralogist, 94, 872-882.

200 Hansen, L.N., Zimmerman, M.E., and Kohlstedt, D.L. (2012) Laboratory measurements of the
201 viscous anisotropy of olivine aggregates. Nature, 492, 415-418.

202 Irifune, T., and Isshiki, M. (1998) Iron partitioning in a pyrolite mantle and the nature of the
203 410-km seismic discontinuity. Nature, 392, 702-705.

- 204 Karato, S.-i. (2011) Water distribution across the mantle transition zone and its implications for
205 global material circulation. *Earth and Planetary Science Letters*, 301, 413-423.
- 206 Kawazoe, T., Nishiyama, N., Nishihara, Y., and Irifune, T. (2010) Deformation experiment at
207 *P-T* conditions of the mantle transition zone using D-DIA apparatus. *Physics of the Earth
208 and Planetary Interiors*, 183, 190-195.
- 209 Kawazoe, T., Ohuchi, T., Nishihara, Y., Nishiyama, N., Fujino, K., and Irifune, T. (2013)
210 Seismic anisotropy in the mantle transition zone induced by shear deformation of
211 wadsleyite. *Physics of the Earth and Planetary Interiors*, 216, 91-98.
- 212 Kubo, T., Ohtani, E., and Funakoshi, K. (2004) Nucleation and growth kinetics of the α - β
213 transformation in Mg_2SiO_4 determined by in situ synchrotron powder X-ray diffraction.
214 *American Mineralogist*, 89, 285-293.
- 215 Keppler, H., and Frost, D.J. (2005) Introduction to minerals under extreme conditions. In R.
216 Miletich, Ed. *Mineral behaviour at extreme conditions*, EMU notes in mineralogy, 7, p.
217 1-30. European Mineralogical Union.
- 218 Libowitzky, E., and Rossman, G.R. (1997) An IR absorption calibration for water in minerals.
219 *American Mineralogist*, 82, 1111-1115.
- 220 Marquardt, H., and Marquardt, K. (2012) Focused ion beam preparation and characterization of
221 single-crystal samples for high-pressure experiments in the diamond-anvil cell. *American
222 Mineralogist*, 97, 299-304.

- 223 Nishihara, Y., Shinmei, T., and Karato, S. (2006) Grain-growth kinetics in wadsleyite: effects of
224 chemical environment. *Physics of the Earth and Planetary Interiors*, 154, 30-43.
- 225 Paterson, M.S. (1982) The determination of hydroxyl by infrared absorption in quartz, silicate
226 glass and similar materials. *Bulletin de Minéralogie*, 105, 20-29.
- 227 Sawamoto, H. (1986) Single crystal growth of the modified spinel (β) and spinel (γ) phases of
228 $(\text{Mg,Fe})_2\text{SiO}_4$ and some geophysical implications. *Physics and Chemistry of Minerals*, 13,
229 1-10.
- 230 Sawamoto, H., and Horiuchi, H. (1990) β $(\text{Mg}_{0.9}, \text{Fe}_{0.1})_2\text{SiO}_4$: Single crystal structure, cation
231 distribution, and properties of coordination polyhedra. *Physics and Chemistry of Minerals*,
232 17, 293-300.
- 233 Shatskiy, A., Litasov, K.D., Matsuzaki, T., Shinoda, K., Yamazaki, D., Yoneda, A., Ito, E., and
234 Katsura, T. (2009) Single crystal growth of wadsleyite. *American Mineralogist*, 94,
235 1130-1136.
- 236 Shimojuku, A., Kubo, T., Ohtani, E., and Yurimoto, H. (2004) Silicon self-diffusion in
237 wadsleyite: Implication for rheology of the mantle transition zone and subducting slabs.
238 *Geophysical Research Letters*, 31, 10.1029/2004GL020002.
- 239 Smyth, J.R., Kawamoto, T., Jacobsen, S.B., Swope, R.J., and Hervig, R.L. (1997) Crystal
240 structure of monoclinic hydrous wadsleyite [β - $(\text{Mg,Fe})_2\text{SiO}_4$]. *American Mineralogist*, 82,
241 270-275.

- 242 Speziale, S., Marquardt, H., and Duffy, T.S. (2014) Brillouin Scattering and its Application in
243 Geosciences. In G.S. Henderson, D.R. Neuville, and R.T. Downs, Eds. Reviews in
244 Mineralogy and Geochemistry, 78, p. 543-603. Mineralogical Society of America,
245 Washington DC.
- 246 Visser, K., Trampert, J., Lebedev, S., and Kennett, B.L.N. (2008) Probability of radial anisotropy
247 in the deep mantle. Earth and Planetary Science Letters, 270, 241-250.
- 248 Wang, J., Bass, J.D., and Kastura, T. (2014) Elastic properties of iron-bearing wadsleyite to 17.7
249 GPa: Implications for mantle mineral models. Physics of the Earth and Planetary Interiors,
250 228, 92-96.

251

252

FIGURE CAPTIONS

- 253 Figure 1. The $(\text{Mg}_{0.89}\text{Fe}_{0.11})_2\text{SiO}_4$ wadsleyite samples synthesized at 16 GPa and 1870 K. **(a)** The
254 sample inside the Re capsule (run H4150). The Re foil was partly removed to show the
255 crystals inside. Two single crystals were also removed at the right part of the sample, and
256 former grain boundaries can be seen as shiny surfaces. The rest of the sample is not shiny
257 because its surface is not smooth due to contact with the capsule wall. **(b)** Examples of the
258 single crystals (run H4150). The crystals look dark because they are thick. Round edges of
259 the crystals reflect the cylindrical shape of the capsule. **(c)** Photomicrograph of a thin section
260 of a single crystal parallel to the (120) plane (run H4015). A few small cracks are visible as
261 gray lines in the left part of the crystal. Note that the whole section does not contain any

262 large inclusions. **(d)** Backscattered electron image of FIB-cut thin section of the single
263 crystal shown in **(c)**.

264 Figure 3. Unpolarized IR absorption spectra of a $(\text{Mg}_{0.89}\text{Fe}_{0.11})_2\text{SiO}_4$ wadsleyite single crystal
265 synthesized at 16 GPa and 1870 K for 1h (run H4015). The crystal platelet was oriented
266 parallel to the (243) plane. A water content of 0.15(1) wt% H_2O ($25000(1000) \text{ H}/10^6 \text{ Si}$) was
267 deduced from 5 measurements at different locations on the same platelet using the Paterson
268 (1982) calibration. All 5 spectra are plotted in this figure to show homogeneity of the water
269 content in the crystal.

270

271

272

273

274

275

276

277

278

279

280

281

Figure 1a

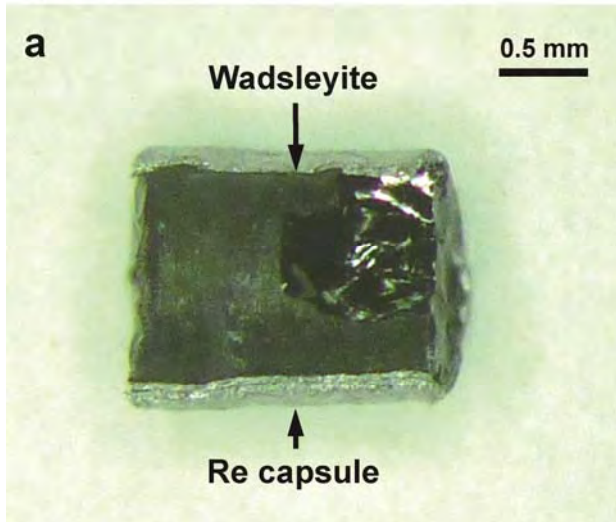
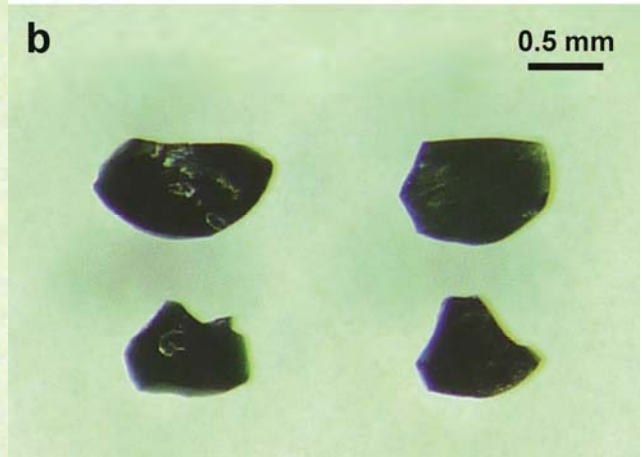


Figure 1b



282

Figure 1c

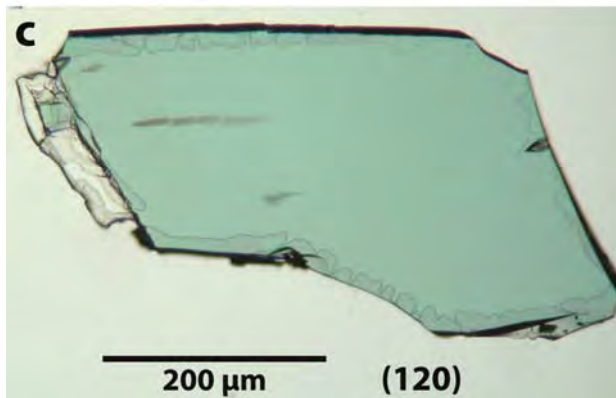
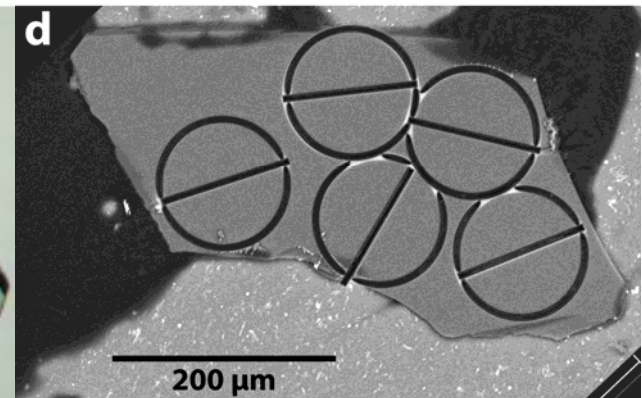


Figure 1d



283

284

285

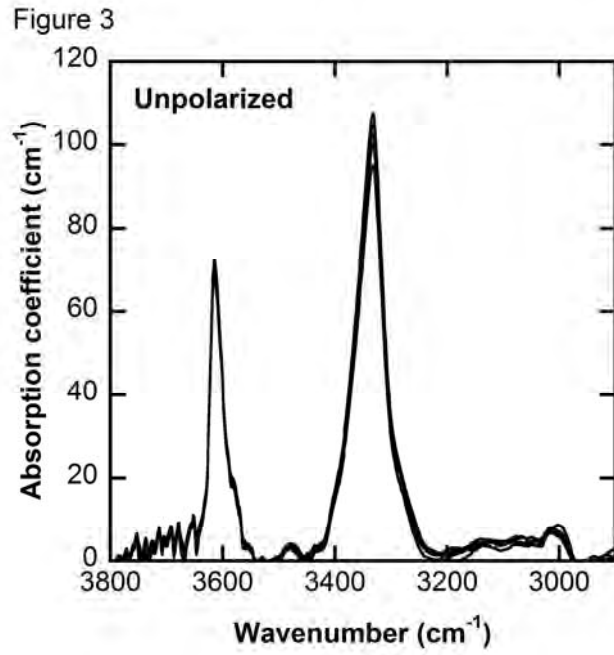
286

287

288

289

290



291